Applied Energy 213 (2018) 235–246

Contents lists available at ScienceDirect

Applied Energy

journal homepage: www.elsevier.com/locate/apenergy

Determining wasted energy in the airside of a perimeter-cooled data center via direct computation of the Exergy Destruction

Luis Silva-Llanca[a,*], Alfonso Ortega[b], Kamran Fouladi[c], Marcelo del Valle[d], Vikneshan Sundaralingam[e]

[a] Universidad de La Serena, Instituto de Investigación Multidisciplinario en Ciencia y Tecnología, Departamento de Ingeniería Mecánica, Benavente 980, La Serena, Chile
[b] Santa Clara University, School of Engineering, 500 El Camino Real, Santa Clara, CA 95053, USA
[c] Wielder University, Department of Mechanical Engineering, 1 University Place, Chester, PA 19013, USA
[d] Villanova University, Laboratory for Advanced Thermal and Fluid Systems, Mechanical Engineering Department, 800 East Lancaster Avenue, Villanova, PA 19085, USA
[e] Internap Corporation, 1 Ravinia Drive, Atlanta, GA 30346, USA

HIGHLIGHTS

- We located and quantified areas of significant airside Exergy Destruction.
- Raised floor pressure drop represented a third of the airside Exergy Destruction.
- The airside encompassed a significant proportion of the overall system losses.

GRAPHICAL ABSTRACT

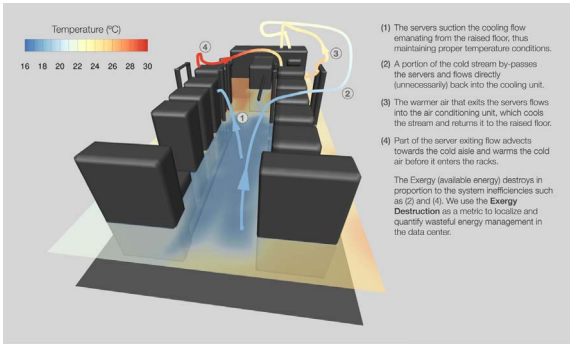

ARTICLE INFO

Keywords:
Energy efficiency
Data center
Exergy destruction
Computational fluid dynamics

ABSTRACT

To keep pace with the growing energy demand, legacy air-cooled data centers begun implementing energy efficiency strategies: Perfecting air flow management, enhancing cooling air delivery and collecting (re-using) waste heat. However, one may wonder: What is the magnitude of these energy savings? Is it worth the effort? The second law of Thermodynamics offers unique insights about energy wasteful practices by estimating the Exergy Destruction in a system. Exergy is equivalent to the "available energy", hence the presence of inefficiencies "Destroys Exergy". In this work, we numerically modeled the behavior of the airside in an existing data center laboratory (CEETHERM) using the commercial Finite Volume software 6SigmaDCX™. The collected numerical data were used to post-process two Exergy Destruction approaches (Direct and Indirect method), whose behavior was tested against: (1) A simplified study case and (2) Actual data center flow. Both approaches worked well against the study case, although for case (2) the Indirect Method–which neglects turbulence effects–predicted zones of artificial negative Exergy Destruction. The Direct Method permitted associating large inefficiencies in the airflow to hot–cold airstream pre-mixing and important pressure drops in the raised floor. The airside Exergy Destruction encompassed a significant amount of the total irreversibilities in the system, suggesting that mitigating (or eliminating) it, can substantially improve energy saving efforts, especially in legacy data centers.

* Corresponding author.
E-mail address: lsilva@userena.cl (L. Silva-Llanca).

https://doi.org/10.1016/j.apenergy.2018.01.031
Received 6 September 2017; Received in revised form 9 January 2018; Accepted 10 January 2018
Available online 28 January 2018

Nomenclature

Symbols

k	turbulence kinetic energy
Pr_t	turbulent Prandtl number
$\dot{Q}_{\mathrm{CRAC}}$	CRAC absorved heat
$\dot{Q}_s$	server dissipating heat
s	specific entropy
$\dot{S}_{gen}$	entropy generation rate
T_0	dead state temperature
T_c	coolant temperature
T_s	server temperature
Tu	turbulence intensity

Greek letters

α_t	turbulent thermal difussivity
ε	turbulence dissipation rate
ν_t	turbulence eddy viscosity
ψ	specific exergy ($\dot{\Psi}/\dot{m}$)
$\dot{\Psi}$	exergy rate
$\dot{\Psi}_d$	Exergy Destruction rate
$\dot{\Psi}'''_d$	Exergy Destruction rate per unit volume
$\dot{\Psi}_{\dot{Q}_t}$	exergy associated with turbulent flux

Subscripts

d	destruction
gen	generation
in	inlet condition
out	outlet condition
ref	reference state

1. Introduction

Between 2007 and 2012, the worldwide data center energy consumption grew at a 4.4% yearly rate [1]; in contrast, the global electricity consumption grew by 3% in the same period. In their study, Van Heddeghem et al. claimed that in 2012 data centers consumed 270 TW h, with the infrastructure electricity such as cooling and power supply losses being the principal consumer at 60% of the total. As opposed to other similar studies, their calculations include servers that draw power but deliver no service, called “orphaned servers”. In terms of absolute electricity use, data centers, communication networks and personal computing each consume roughly the same power; the authors mentioned this to recommend energy-efficiency research throughout those three categories.

Most traditionally designed data centers utilize underfloor air cooling in which the conditioned air emanates from the main CRAC/CRAH unit via the underfloor space then through perforated tiles into a so-called “cold aisle” between two rows of racks, Fig. 1. The server fans suction this cooling air and reject it at an elevated temperature into the “hot aisle”. The flow returns via the overhead space to the CRAC unit.

The large power consumption associated with HVAC in data centers, renders thermal management as key towards efficient operation. Several studies have presented a variety of energy saving techniques, such as: Cooling and IT equipment redistribution, liquid cooling, localized cooling, aisle containment, airside economization [2–17]. Rambo and Joshi [16] analyzed different cooling configurations, recommending what they called the “OH-RR” (overhead supply and room return) scheme with the CRAC units opposing each other in the room. The Rack Cooling Index (RCI), introduced by Herrlin [17], improves the cooling effectiveness assessment in data center design. The author highlighted the shortcomings of solely using the temperature distribution to rank different designs.

Computational Fluid Dynamics (CFD) in data centers appears as a convenient tool for rapid design and diagnosis [3,7,10,13,16,18–30]. Compared to empirical investigations, CFD allows studying the data center airside cooling flow in great detail and, when done accurately, it leads to more intelligent decision making. Previous studies favored the Finite Volume Method as their numerical approach and the k-ε model to represent the turbulence [3,7,10,16,18,20,21,23–25,27–30].

A portion of data center thermodynamic analyses made use of the Exergy Destruction as a way to quantify inefficiencies [2,24,31–35]. In general, those studies followed a clasical thermodynamic approach by assuming the cooling components in mechanical and thermal equilibrium (uniform velocity and temperature distributions), including the complex air flow inside the server room. One exception, Shah et al. [24], simulated and quantified the pre-mixing of cold air with leaking air from the hot aisle in terms of Exergy loss, although they neglected pressure drop and turbulence effects. The study expanded to the rest of the data center components, where they compared individual to overall inefficiencies.

2. Motivation and objectives

Prior studies demonstrated that nearly a third of the Exergy supplied to the data center vanishes due to unoptimized thermal management [24]. Estimating the Exergy Destruction in the data center airspace appears as a practical metric to localize and quantify inefficiencies due to inadequate server cooling.

Common practice in Exergy Destruction computations establishes the Exergy balance and estimates the Exergy Destruction as the imbalance in that equation. Kock and Herwig [36] coined the term “Indirect Method” to define this approach, as the Exergy Destruction is calculated indirectly from other quantities such as entropy and heat fluxes. Kock and Herwig [37] proposed a second method to measure the Exergy Destruction by directly computing it from the velocity and temperature fields, the “Direct Method”. They demonstrated the superiority of the Direct Method and recommended its use in complex flow scenarios.

This study aims to identify and accurately quantify wasteful cooling in a perimeter-cooled data center airspace, including an examination of the role of viscous dissipation (pressure drop) which heretofore has always been assumed to be negligibly small in data center airflows. Furthermore, we directly compute the detrimental effect that turbulence exerts over the system efficiency; also neglected in prior studies. We also perform a side by side comparison of the Direct and Indirect

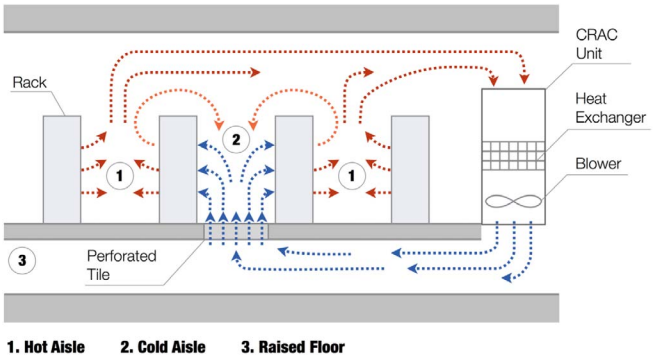

Fig. 1. Fluid flow schematic in a perimeter cooled data center.

approaches in the context of a data center airspace CFD. To the best of our knowledge, no previous studies applied the Direct Method in air cooled data center simulations.

3. Mathematical model and numerical implementation

3.1. Exergy Destruction analysis for steady state numerical simulations (Indirect method)

Although the numerical formulation includes the three dimensions, for the sake of simplicity, the mathematical modeling henceforth will remain two-dimensional. Fig. 2 represents any given section inside a computational domain, with one face centered at P and its neighboring cells centered at W, E, S and N. An Energy and Entropy balance inside the central volume (gray area) yields [38]:

$$0 = -(\dot{m}h + \dot{Q})_{\mathrm{w}} + (\dot{m}h + \dot{Q})_{\mathrm{e}} - (\dot{m}h + \dot{Q})_{\mathrm{s}} + (\dot{m}h + \dot{Q})_{\mathrm{n}} \tag{1}$$

$$\dot{S}_{gen} = -\left(\dot{m}s + \frac{\dot{Q}}{T}\right)_{\mathrm{w}} + \left(\dot{m}s + \frac{\dot{Q}}{T}\right)_{\mathrm{e}} - \left(\dot{m}s + \frac{\dot{Q}}{T}\right)_{\mathrm{s}} + \left(\dot{m}s + \frac{\dot{Q}}{T}\right)_{\mathrm{n}} \tag{2}$$

where $\dot{Q}$ and $\dot{m}$ are the heat and mass fluxes the direction normal to the cell face, respectively. The sub-indices w,e,s and n represent the cell boundaries corresponding to the adjacent face of the same letter (Fig. 2). The Gibbs equation for an ideal gas can be integrated from an arbitrary reference state (that ultimately cancels out); for example, for the west face:

$$s_{\mathrm{w}} - s_{ref} = c_p \ln(T_{\mathrm{w}}/T_{ref}) - R\ln(P_{\mathrm{w}}/P_{ref}) \tag{3}$$

The Exergy Destruction can be defined in terms of the Entropy Generation and the dead state temperature T_0 as:

$$\dot{\Psi}_{d_i} = T_0 \dot{S}_{gen_i} = T_0 \left\{ -\sum_{\mathrm{w,s}} \dot{m}_j \left[c_p \ln\left(\frac{T_j}{T_0}\right) - R\ln\left(\frac{P_j}{P_0}\right)\right] - \sum_{\mathrm{w,s}} \frac{\dot{Q}_j}{T_j} + \sum_{\mathrm{e,n}} \dot{m}_j \left[c_p \ln\left(\frac{T_j}{T_0}\right) - R\ln\left(\frac{P_j}{P_0}\right)\right] + \sum_{\mathrm{e,n}} \frac{\dot{Q}_j}{T_j} \right\} \tag{4}$$

The arbitrary reference state, can be chosen as equal to the dead state to simplify the calculations. By adding the Exergy Destruction estimated in each cell, we obtain the total Exergy Destruction in the system $\sum \dot{\Psi}_{d_i}$.

$$\dot{\Psi}_{d_{total}} = \sum \dot{\Psi}_{d_i} \tag{5}$$

This method is called "Indirect" since it estimates $\dot{\Psi}_d$ by equating it to the rest of the terms in the Second Law balance (2). In other words, this approach defines $\dot{\Psi}_d$ as the summation of what imbalances the Exergy transport in the system.

3.2. Comparison with best practices in data center Exergy analysis

Fig. 3 depicts a control volume subject to generalized physics, which leads to the expression proposed by Shah et al. [24]:

$$\dot{\Psi}_d = \sum_j \left(1 - \frac{T_0}{T_j}\right)\dot{Q}_j - \dot{W}_{\mathrm{cv}} + \sum_{\mathrm{in}} \dot{m}_i \left[(h - h_0) + \frac{V^2}{2} + g(z - z_0) - T_0(s - s_0)\right]_{\mathrm{in}} - \sum_{\mathrm{out}} \dot{m}_o \left[(h - h_0) + \frac{V^2}{2} + g(z - z_0) - T_0(s - s_0)\right]_{\mathrm{out}} \tag{6}$$

The following assumptions simplify the latter equation: (1) $\dot{W}_{cv}$ represents the boundary work, which vanishes since the cell boundaries are static, and (2) $\dot{Q}_0 = 0$ since the cells inside the numerical domain transfer no heat to the environment. Arbitrariness exists in the choice of T_0, thus care must be taken in its choice so as to assure consistency between different studies.

Eq. (6) can be re-arranged as:

$$\dot{\Psi}_d = \overbrace{\sum_j \dot{Q}_j + \dot{m}_i h^+_{\mathrm{in}} - \dot{m}_o h^+_{\mathrm{out}}}^{=0} + T_0 \left(-\sum_j \frac{\dot{Q}_j}{T_j} - \dot{m}_i [s - s_0]_{\mathrm{in}} + \dot{m}_o [s - s_0]_{\mathrm{out}} \right) \tag{7}$$

where $h^+ \equiv (h - h_0) + V^2/2 + g(z - z_0)$. The first three terms in Eq. (7) sum to zero because of the energy balance (Eq. (1)), and should be eliminated from the formulation as they can introduce unnecessary numerical inaccuracies due to computational errors (e.g., round-off, truncation). Re-stating Eq. (7):

$$\dot{\Psi}_d = T_0 \left(\dot{m}_o [s - s_0]_{\mathrm{out}} - \dot{m}_i [s - s_0]_{\mathrm{in}} - \sum_j \frac{\dot{Q}_j}{T_j} \right) \tag{8}$$

The consistency between Eqs. (8) and (4) proves that the two formulations should result in the same outcome.

3.3. Alternative approach for the Exergy Destruction computation (Direct method)

Kock and Herwig [36,37,39] introduced an approach to directly compute the Entropy Generation in turbulent flows, the so-called "Direct Method", as follows [37]:

$$\dot{S}'''_{gen} = \underbrace{\frac{\mu}{\overline{T}} \left\{ 2\left[\left(\frac{\partial \overline{u}}{\partial x}\right)^2 + \left(\frac{\partial \overline{v}}{\partial y}\right)^2 \right] + \left(\frac{\partial \overline{u}}{\partial y} + \frac{\partial \overline{v}}{\partial x}\right)^2 \right\}}_{\dot{S}'''_{gen,\overline{D}}} + \underbrace{\frac{\lambda}{\overline{T}^2} \left[\left(\frac{\partial \overline{T}}{\partial x}\right)^2 + \left(\frac{\partial \overline{T}}{\partial y}\right)^2 \right]}_{\dot{S}'''_{gen,\overline{C}}} + \underbrace{\frac{\mu}{\overline{T}} \left\{ 2\left[\overline{\left(\frac{\partial u'}{\partial x}\right)^2} + \overline{\left(\frac{\partial v'}{\partial y}\right)^2} \right] + \overline{\left(\frac{\partial u'}{\partial y} + \frac{\partial v'}{\partial x}\right)^2} \right\}}_{\dot{S}'''_{gen,D'}} + \underbrace{\frac{\lambda}{\overline{T}^2} \left[\overline{\left(\frac{\partial T'}{\partial x}\right)^2} + \overline{\left(\frac{\partial T'}{\partial y}\right)^2} \right]}_{\dot{S}'''_{gen,C'}} \tag{9}$$

where λ and μ are the thermal conductivity and the dynamic viscosity, respectively. The four terms in (9) can be individualized according to their contribution as:

1. $\dot{S}'''_{gen,\overline{D}}$: entropy generation by direct (mean flow) dissipation.
2. $\dot{S}'''_{gen,D'}$: entropy generation by turbulent dissipation.
3. $\dot{S}'''_{gen,\overline{C}}$: entropy generation by heat conduction.
4. $\dot{S}'''_{gen,C'}$: entropy generation by turbulent heat transfer with fluctuating

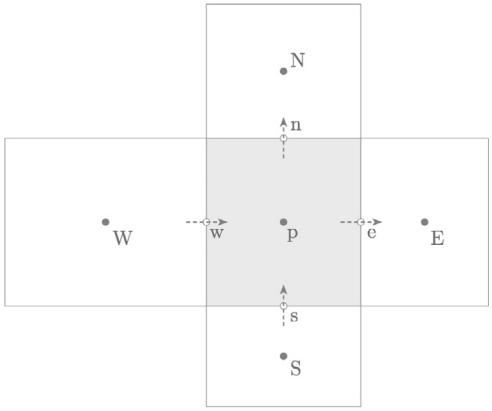

Fig. 2. Control volume and its neighboring cells for a steady state two-dimensional numerical simulation.

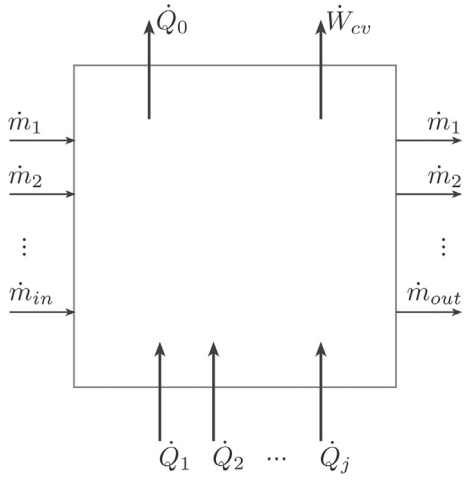

Fig. 3. Generalized control volume with multiple heat flows, mass inflows and outflows.

temperature gradients.

The computation of the second and fourth terms depends on the turbulent model used. Kock and Herwig [37] defined $\dot{S}'''_{gen,D'}$ and $\dot{S}'''_{gen,C'}$ as functions of the kinetic energy k and the rate of viscous dissipation ε:

$$\dot{S}'''_{gen,D'} = \frac{\rho\varepsilon}{\overline{T}} \tag{10}$$

$$\dot{S}'''_{gen,C'} = \frac{\alpha_t}{\alpha}\frac{\lambda}{\overline{T}^2}\left[\left(\frac{\partial\overline{T}}{\partial x}\right)^2 + \left(\frac{\partial\overline{T}}{\partial y}\right)^2\right] \tag{11}$$

where $\alpha_t = \nu_t/Pr_t$ and $\nu_t = C_\mu k^2/\varepsilon$; the kinetic energy k and the rate of viscous dissipation ε are known as they are part of the system of equations solved by the CFD code. Further details and the complete 3-D formulation may be found in [37].

Finally, we obtain the Exergy Destruction such that:

$$\dot{\Psi}'''_d = T_0\dot{S}'''_{gen} \tag{12}$$

Although Eqs. (9)–(11) seem a priori complex to compute, current CFD tools offer convenient access to field variables (velocity, pressure, temperature) and their derivatives, which greatly simplifies the Exergy Destruction calculation for rapid engineering design.

3.4. Implementation of the indirect and direct method within CFD framework

The Navier-Stokes equations were solved via the k-ε model using commercially available software, either 6SigmaDCX™ or ANSYS Fluent™. Once the CFD code finds its convergence, the relevant variables are imported into an ad hoc numerical code written in Matlab™ to post-process the Exergy Destruction (Entropy Generation), as shown schematically in Fig. 4. The velocities, temperatures and turbulent quantities extracted from the CFD approach exist at the control volume corners (Fig. 2), hence the post processing technique required for the variables to be interpolated towards the cell centers (gray dots) or the cell faces (white dots); all interpolations were implemented as linear. It is important to remark that in a non-uniform grid, as used in most CFD analyses, the face is not equidistant to the adjacent nodes: $x_w \neq 0.5\cdot(x_p + x_W)$. This issue has to be taken into account especially when mass and heat fluxes need to be accurately calculated at the cell faces.

For the Indirect Method, each term in Eq. (4) is evaluated at its corresponding cell face. The heat flux and mass flow rate passing through the face w of area A_x are computed as:

$$\dot{Q}_w = -\lambda A_x\frac{T_w - T_W}{x_w - x_W}, \qquad \dot{m}_w = \rho A_x u_w \tag{13}$$

The analysis for the remainder of the cell faces (e,s,n) is analogous.

The Direct Method, described in Eqs. (9)–(11), only requires information from the central control volume (gray area in Fig. 2), thus requiring fewer interpolations than the Indirect Method and rendering it more computationally efficient. The variables $\overline{T}$,k and ϵ are evaluated at the cell center P, whereas the gradients are estimated with second-order accuracy using central differences in terms of the face values. For example, the temperature gradient with respect to x is calculated as:

$$\frac{\partial\overline{T}}{\partial x} = \frac{T_e - T_w}{x_e - x_w} \tag{14}$$

3.5. Direct and Indirect method against a study case

A well investigated experimental data set is used to validate the Exergy Destruction computations. This section focuses solely on the computation of $\dot{\Psi}_d$; the intention is to validate the ad hoc numerical approach, rather than the previously established mathematical approach.

Fig. 5 illustrates the physical situation for the study case. The fluid flows between two parallel plates in the turbulent regime, subject to a constant heat flux per unit length q'_{wall}. We use an Entropy Generation formulation (Bejan [40]) in terms of the bulk properties of the flow to subsequently compute the Exergy Destruction (similarly to Eq. (4)):

$$\dot{\Psi}'_d = \frac{T_0 q'^2_{wall}}{4T^2\dot{m}c_p}\frac{D}{St} + \frac{2T_0\dot{m}^3}{\rho^2 T}\frac{f}{DA^2} \tag{15}$$

where D is the hydraulic diameter, $\dot{m}$ is mass flow rate, A is the cross-sectional area and the Stanton number St = Nu/(Re Pr). The friction factor f and the Nusselt number Nu can be obtained as functions of Re through experimental data correlation [41]:

$$\mathrm{Nu} = 0.0539\,\mathrm{Re}^{0.704}, \quad f = 0.11\,\mathrm{Re}^{-0.276} \tag{16}$$

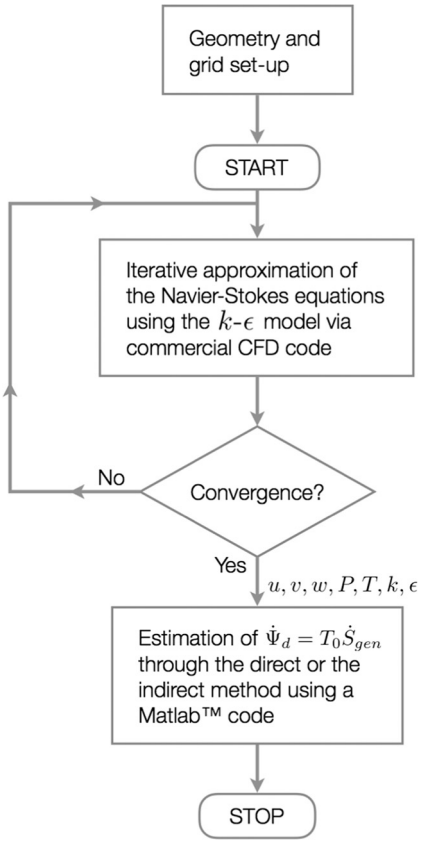

Fig. 4. Sequence of operations to compute the Exergy Destruction.

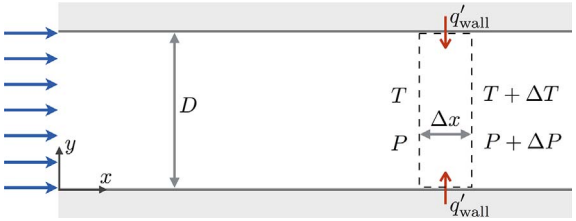

Fig. 5. Schematic for the study case.

Eq. (15) can be rewritten in terms of Re as:

$$\dot{\Psi}'_d = \underbrace{4.638\frac{T_0 {q'_{wall}}^2 D^2}{T^2 A \lambda}\mathrm{Re}^{-0.704}}_{\dot{\Psi}'_{d,\Delta T}} + \underbrace{0.22\frac{T_0 A \mu^3}{\rho^2 T D^4}\mathrm{Re}^{2.724}}_{\dot{\Psi}'_{d,\Delta P}} \tag{17}$$

The first term in Eq. (17) relates to Exergy Destruction due to heat transfer ($\dot{\Psi}'_{d,\Delta T}$), whereas the second term accounts for viscous dissipation (friction) effects $\dot{\Psi}'_{d,\Delta P}$. It can be inferred that $\dot{\Psi}'_{d,\Delta T}$ decreases with increasing Re as the heat transfer at the wall improves due to the augmentation of the flow rate. On the other hand, $\dot{\Psi}'_{d,\Delta P}$ is directly proportional to Re due to the increase in fluid friction leading to larger pressure drop. This competing effect of Re over $\dot{\Psi}'_d$ suggests the existence of optimum conditions where $\dot{\Psi}'_d$ minimizes:

$$\mathrm{Re}_{opt} = 1.639\left(\frac{\rho\, {q'_{wall}}^2 D^3}{\mu^{1.5}(\lambda\, T)^{0.5}}\right)^{0.583} \tag{18}$$

The numerical simulation was performed using ANSYS Fluent™, via the standard *k*-ε model with enhanced wall treatment. Due to the large velocity and temperature gradients in turbulent flows, the mesh point nearest to the wall was set to be approximately at $y^+ = 1$. For this internal flow, the numerical accuracy depends mostly on how well the code solves the flow and heat transfer in the vicinity of the wall. The computational domain is set to be sufficiently long for the flow to fully develop.

The control volume bounded by dashed lines shown in Fig. 5 was used to estimate $\dot{\Psi}'_d$ from the numerical data in two ways:

1. Integral Control Volume Approach: Following an analogous procedure that led to Eq. (4) applied to the integral control volume shown in Fig. 5 yields:

$$\dot{\Psi}'_d = \frac{T_0 \dot{m}}{\Delta x}\left[c_p \ln\left(1+\frac{\Delta T}{T}\right) - R\ln\left(1+\frac{\Delta P}{P}\right)\right] - 2T_0\frac{q'_{wall}}{T_{wall}} \tag{19}$$

   where T_{wall} is the wall surface temperature at which the heat flux crosses the control volume.
2. Differential Control Volume Approach: Entropy generation summation of each cell inside the control volume using either the indirect (Eq. (4)) or direct (Eq. (9)) method:

$$\dot{\Psi}'_d = \sum_i (\dot{\Psi}'''_d\, \Delta y\, \Delta z)_i \tag{20}$$

In this 2-D analysis, Δz was considered equal to unity.

The Exergy Destruction per unit length as a function of Re is shown in Fig. 6. The integral CV approach (Eq. (19)) deviates from the empirical method between 5 and 15%, whereas the direct and indirect differential CV methods deviate between 10 and 20%. When using the *k*-ε model, deviations below 25% are considered adequate enough. Compared to the empirical data, the numerical approaches followed a similar trend, finding optimality near $\mathrm{Re} \approx 1.5 \times 10^5$.

The integral CV approach under-predicts at low Re, although the curves tend to converge as Re increases. Kock [37] and Herwig and Kock [36] presented similar data for turbulent internal pipe flow using direct numerical simulation (DNS), observing a similar trend for low and high Re, with deviations ranging between 12 and 75%. Herwig and Kock [36] proposed an explanation for this disagreement, where they re-arranged the transport equation for Entropy, such that:

$$\dot{S}'''_{gen} = \underbrace{\overline{\frac{\lambda}{T^2}(\nabla T)^2} + \overline{\frac{\mu}{T}\Phi}}_{\text{Generation}} = \underbrace{\rho\frac{\overline{Ds}}{Dt}}_{\text{Convection}} - \underbrace{\overline{\nabla\cdot\frac{q}{T}}}_{\text{Molecular flux}} + \underbrace{\rho\left(\frac{\partial\overline{u's'}}{\partial x} + \frac{\partial\overline{v's'}}{\partial y} + \frac{\partial\overline{w's'}}{\partial z}\right)}_{\text{Turbulent flux}} \tag{21}$$

The third term on the right hand side corresponds to the Turbulent Entropy Flux, which can be modeled analogously to the turbulent heat flux in the energy equation [36]:

$$\rho\left(\frac{\partial\overline{u's'}}{\partial x} + \frac{\partial\overline{v's'}}{\partial y} + \frac{\partial\overline{w's'}}{\partial z}\right) = -\overline{\nabla\cdot\left(\frac{q}{T}\right)_t} \tag{22}$$

In prior studies [36,37,40] the authors neglected the turbulent entropy flux, assuming that its contribution is insignificant near the wall and between the inlet and outlet of a given control volume inside the domain. This assumption resembles neglecting $\mathrm{d}T/\mathrm{d}x$ in internal flows using scaling analysis. Herwig [36] claimed that this assumption is valid for high Re, which explains the disagreement in the data for low Re. The integration of the right hand side of Eq. (21) over the control volume shown in Fig. 5, leads to Eq. (4), as long as the entropy turbulent flux is ignored.

In summary, both the direct and indirect differential approaches are consistent with each other and predict results that adequately compare with the integral approach. However, neglecting the turbulent flux term in the indirect method generates inconsistencies for typical data center air-flow, as discussed in the following section.

4. Direct and indirect method in data center airside flow

4.1. Numerical and experimental procedure

The simulated 111.5 m^2 data center corresponds to the CEETHERM Laboratory located at The Georgia Institute of Technology, which comprises 7 operating racks and five cooling components: A downflow Liebert Computer Room Air Conditioning Unit (CRAC), a downflow Liebert CRAC unit with air-side economizer, an upflow Liebert CRAC and two in-row coolers. Fig. 7 depicts the computer generated representation of the CEETHERM laboratory as used in the simulations. The numerical model was assumed in steady state, since the temperature and power measurements demonstrated negligible time variation. The raised floor has a 0.91 m depth, whereas the false ceiling (return duct) is 0.76 m from the ceiling slab. The data center Racks and CRAC unit operating conditions are detailed in Tables 1 and 2, respectively.

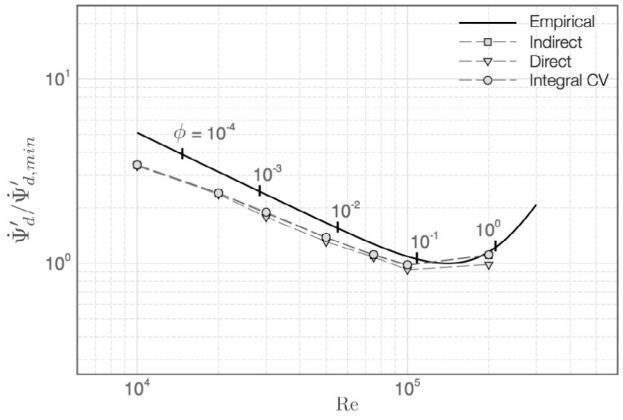

Fig. 6. Normalized Exergy Destruction vs Reynolds number.

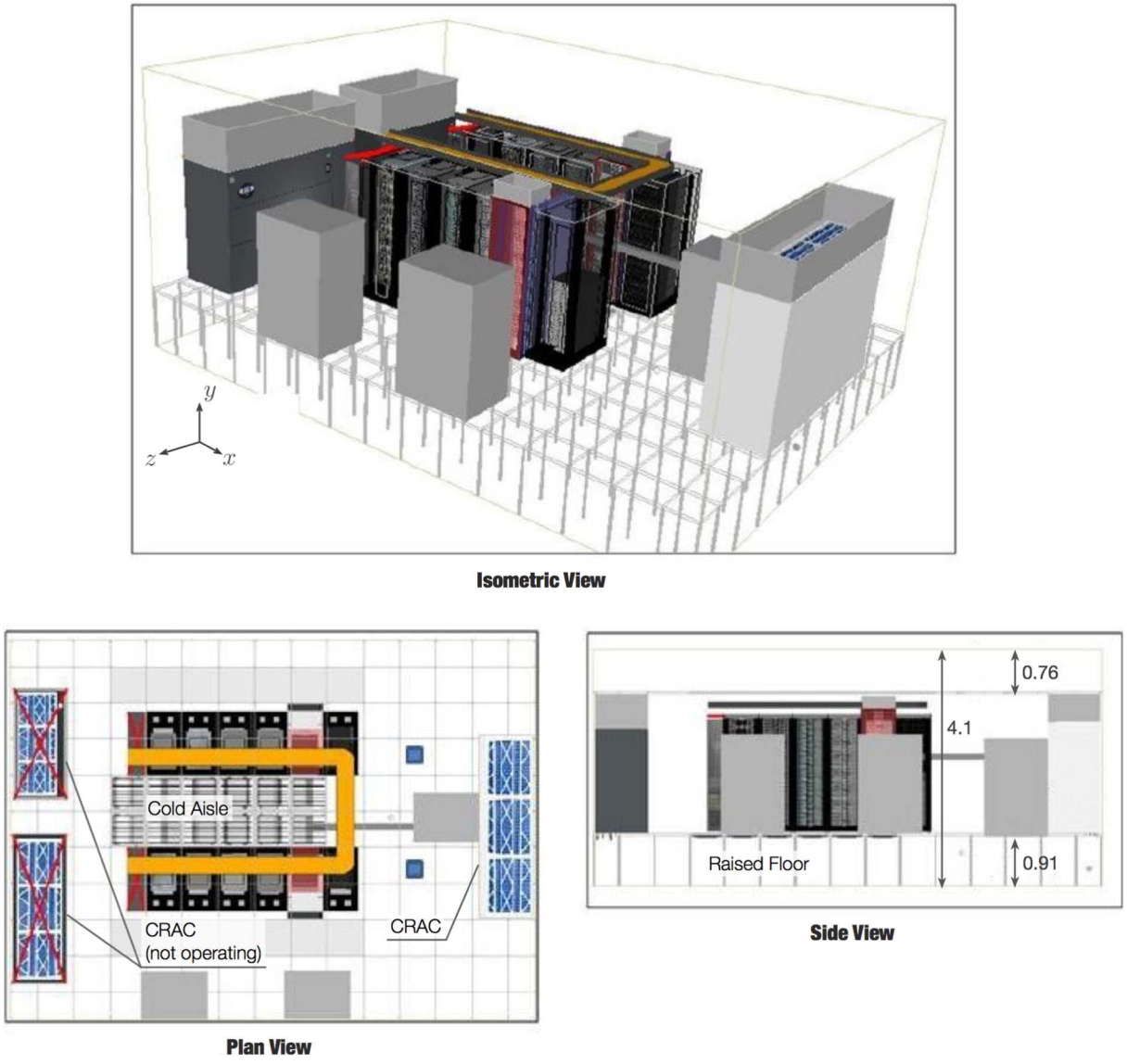

Fig. 7. CEETHERM CAD model utilized in the computations (units in meters).

Table 1
Racks operating conditions.

Rack	Inlet T (°C)	Outlet T (°C)	Flow rate (CFM)	Power (kW)
1	19.0	27.5	1557	7.43
2	18.4	24.7	1472	5.27
3	18.6	24.4	1646	5.37
4	21.0	26.7	1646	5.37
5	19.5	25.3	1646	5.37
6	19.2	24.7	1559	4.87
7	23.2	37.6	1538	12.5

Table 2
CRAC operating conditions.

Inlet T (°C)	Inlet T (°C)	Flow rate (CFM)	Net cooling (kW)	Power consumption (kW)
24.4	17.4	12,900	51.1	7.46

The heat transfer and fluid flow inside the data center was simulated using a finite volume approach via the commercial code 6SigmaDCX™. The flow regime was assumed as turbulent and represented by the standard k-ε model, with constant properties of air. The model assumes a complete conversion of IT power into heat (46.2 kW).

The temperature measurements were carried through a mobile grid of 252 type T thermocouples. The rig allowed its displacement inside the cold and the two hot aisles, delivering a three-dimensional temperature distribution. The data reported an uncertainty in the vicinity of ± 0.5 °C. More details in the experimental and numerical implementation may be found in [42].

The deviation between the numerical and experimental data δ was calculated as the difference between the simulated temperature field T_{num} and the measured temperature T_{exp}, leading to the following expression:

$$\delta = T_{num} - T_{exp} \tag{23}$$

Fig. 8 shows the distribution of δ within the domain including three view planes. In order to compute Eq. (23), the numerical data were interpolated to the exact location of each thermocouple measurement.

A mesh with approximately 1.5 million nodes proved sufficient to adequately represent the physics. The mean temperature deviation $\overline{\delta}$ and its standard deviation σ were used to compare five different mesh densities, ranging from 128,154 to 2,258,766 nodes, as shown in Table 3. The deviations presented marginal differences when the

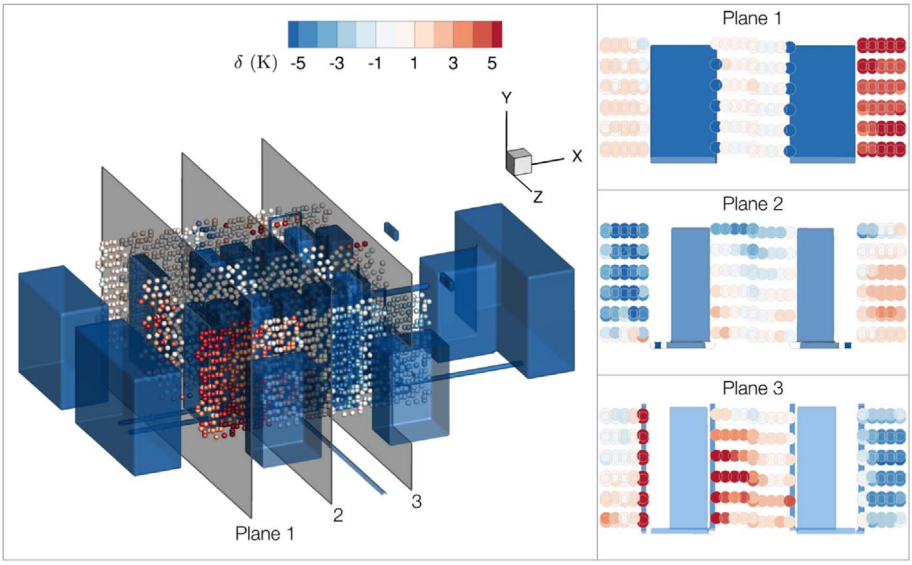

Fig. 8. Numerical data deviation with respect to experimental temperature measurements inside CEETHERM data center.

Table 3
Mean temperature deviation $\bar{\delta}$ and its standard deviation σ for different grid sizes in the left (HAA), right (HAB) and cold (CA) aisles.

Mesh	N of elements	$\bar{\delta}_{HAL}$	$\sigma_{\delta HAL}$	$\bar{\delta}_{CA}$	$\sigma_{\delta CA}$	$\bar{\delta}_{HAR}$	$\sigma_{\delta HAR}$
1	2,258,766	1.68	1.72	1.56	1.75	3.24	1.81
2	1,447,218	1.74	1.75	1.32	1.60	3.26	1.78
3	622,440	1.81	1.71	1.34	1.61	2.97	1.70
4	211,968	1.77	1.76	1.37	1.25	3.07	1.89
5	128,154	1.79	1.54	1.38	1.42	2.79	1.84

number of nodes was augmented, demonstrating robustness in the numerical approach, at least within the measured areas (hot and cold aisles). The second most dense mesh (1,447,218 nodes) required a CPU time of approximately 10 min using 30 processors running in parallel; its low computational time and good accuracy led us to chose this configuration for the rest of the calculations.

In general, the data showed good agreement ($|\delta| < 2$ K), with some higher underprediction (blue data) in the order of 4–5 K in the center plane (Fig. 8). Similarly, the cold aisle presented good agreement overall, with overprediction (red data) in the end closer to the CRAC Unit (Plane 3). The right hot aisle proved to be a more complicated zone to predict, showing overprediction and underprediction, particularly towards the aisle ends (Plane 1 and 3).

4.2. Superiority of the Direct Method in data center flow

The Indirect Method, as defined in (4), artificially introduced zones of negative Exergy Destruction. Fig. 9 compares the direct and indirect methods by depicting the distribution of the Exergy Destruction per unit volume $\dot{\Psi}_d'''$ inside CEETHERM. Both approaches presented similar values in magnitude, although their distributions differed in the prominent blue areas ($\dot{\Psi}_d''' < 0$) generated by the indirect method (Fig. 9(a)). We believe that this inconsistency, which violates the

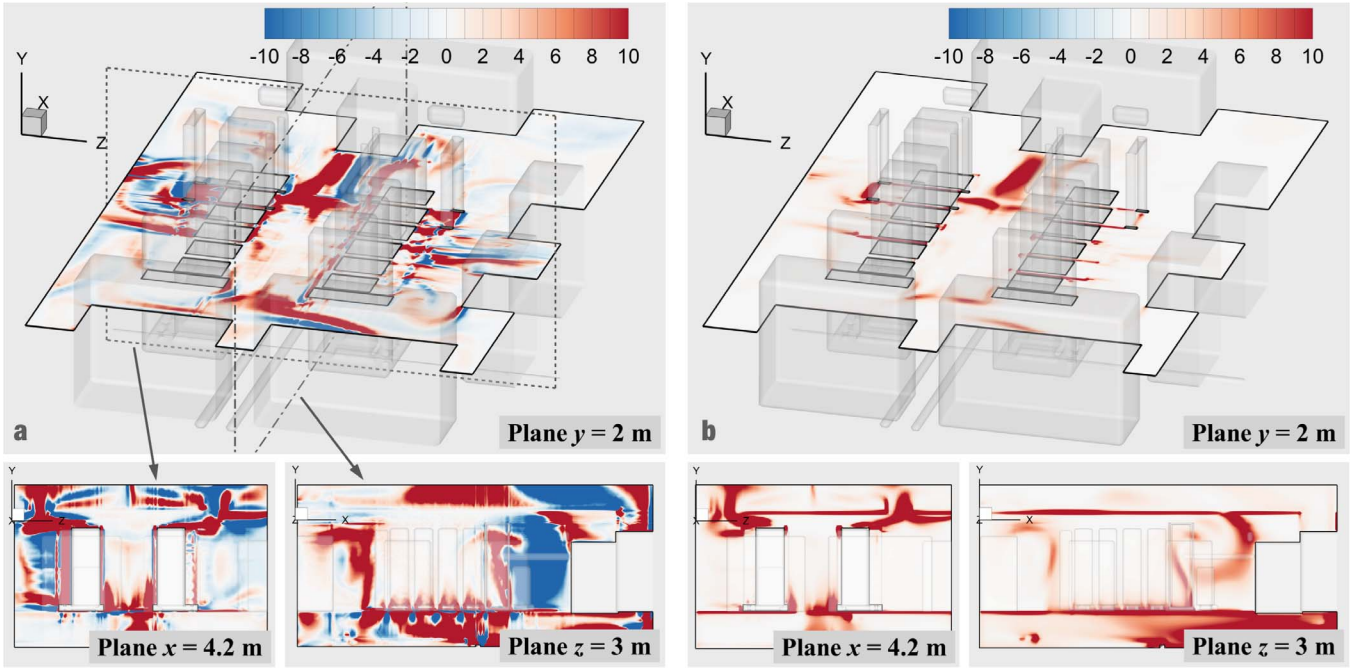

Fig. 9. Exergy Destruction per unit volume inside CEETHERM, for three different views. (a) Eq. (4); (b) Eq. (9).

second law of thermodynamics, relates to the exclusion of the turbulent flux terms in Eq. (21).

Herwig and Kock [36] tested the direct and indirect method (also neglecting the turbulent flux terms) over two cases: (1) Fully developed pipe flow under constant heat flux and (2) Pipe flow with an inserted twisted tape that promotes turbulence and improves the heat transfer. They found differences between the two approaches, especially for case 2, attributed to two main reasons:

(a) Ignoring the terms associated with heat flux at the inlet and outlet boundaries holds valid only at sufficiently large Reynolds numbers. Even small data centers, such as CEETHERM, present numerous inlet and outlet boundaries, namely the racks and the cooling units, complicating a truly representative definition of Re. Moreover, because of the nonuniform distribution of the velocity entering and exiting each server, we expect the assumption to occasionally work, since Re likely ranges from large to small across racks.
(b) Neglecting the turbulent flux terms in Eq. (4) generates inaccuracies when the flow and temperature fields considerably differ between inlets and outlets. Such conditions typically appear in data center air-flow, in fact, as stated before we hypothesize this as the main reason as to why the indirect method failed (Fig. 9(a)).

The Turbulence Intensity indicates the level of turbulent fluctuation in the velocity field with respect to the main flow, defined as [43]:

$$\mathrm{Tu} = \frac{\sqrt{1/3(\overline{u'^2} + \overline{v'^2} + \overline{w'^2})}}{U_0} = \frac{\sqrt{2k/3}}{U_0} \tag{24}$$

Where the characteristic velocity U_0 was selected as the mean velocity passing through the tiles.

The distribution of Tu inside CEETHERM (Fig. 10) reinforces the hypothesis that the turbulence flux terms matter in data center airside flow. Let us recall that the Direct Method (Fig. 9(b)) represents a complete formulation of the Exergy Destruction, meaning that it includes the turbulence contribution to the overall irreversibilities. Comparing Figs. 9(a) and 10 evidences the direct proportionality between the problematic zones ($\dot{\Psi}'''_d < 0$) and Tu.

Although a qualitative correlation between two variables ($\dot{\Psi}'''_d$ and Tu) lacks conclusiveness, it nonetheless presents a strong case for the turbulence flux terms important influence over $\dot{\Psi}'''_d$.

5. Airside Exergy Destruction within the overall data center Exergy exchange

5.1. Decomposing inefficiencies due to inadequate heat transfer and pressure drop

Table 4 contrasts every Exergy Destruction term in the Direct Method, with viscous dissipation (pressure drop) accounting for approximately 36%. The terms related to turbulent fluctuations ($\dot{\Psi}_{d,D'}$ and $\dot{\Psi}_{d,C'}$) dominated the total Exergy Destruction, demonstrating the magnitude of error introduced when neglecting turbulence.

Fig. 11 compares the Exergy Destruction distribution with the pressure and temperature fields by depicting: (a) Entropy Generation due to viscous dissipation $\dot{\Psi}'''_{d,D}$, (b) Entropy Generation due to conduction $\dot{\Psi}'''_{d,C}$, (c) Pressure field, (d) Temperature field and a few streamlines to indicate flow directionality. The figure presents views oriented perpendicular to the *y*,*x* and *z* axes, each providing insight as to what causes the airside irreverisibilities and how they distribute inside the data center as follows:

Plane *y*: Fig. 11(d) shows that fluid from the cold aisle (blue[1] area) advects towards the CRAC unit, where it mixes especially with warmer air at ≈ 30 °C. This inefficiency manifests as an irreversibility, as demonstrated by Fig. 11(b) where the aforementioned cold-warm air mixing zone coincides with the largest zone of Exergy Destruction. By comparing Fig. 11(a) and (b), the majority of $\dot{\Psi}'''_d$ in this plane view appears due to heat conduction, as viscous dissipation effects appeared mostly within the raised floor.

Plane *x*: Notable viscous dissipation effects in the floor plenum emerge due to the large pressure drop that the airflow suffers as it forces through the perforated tiles (Fig. 11(a) and (c)). Fig. 11(d) shows fluid from the cold aisle (blue) "leaking" over the top of both racks, mixing with warmer air from the hot aisles. This effect generates sufficiently large temperature gradients such that two plumes with high $\dot{\Psi}'''_d$ rise over the top of each hot aisle (Fig. 11(b)).

Plane *z*: This view permits correlating $\dot{\Psi}'''_d$ to raised floor airflow (Fig. 11(a)), especially near the CRAC unit. In this case, the downward cooling flow exiting the CRAC unit suddenly turns horizontally towards the cold aisle, which generates a significant pressure drop. Cold aisle air leaking happens in the vicinity of the cooling units, where two recirculating streamlines show that the colder fluid advects downward, subsequently mixing with warmer air coming from the hot aisles (Fig. 11(d)). Fig. 11(b) corroborates this observation, where two zones of significant $\dot{\Psi}'''_d$ appear near the cooling units.

The Exergy Destruction distribution inside a data center room provides information about the critical zones that require attention during design and/or operation. Since this technique also quantifies inefficiencies in Watts, it can be potentially combined with economic analysis for more comprehensive decision making.

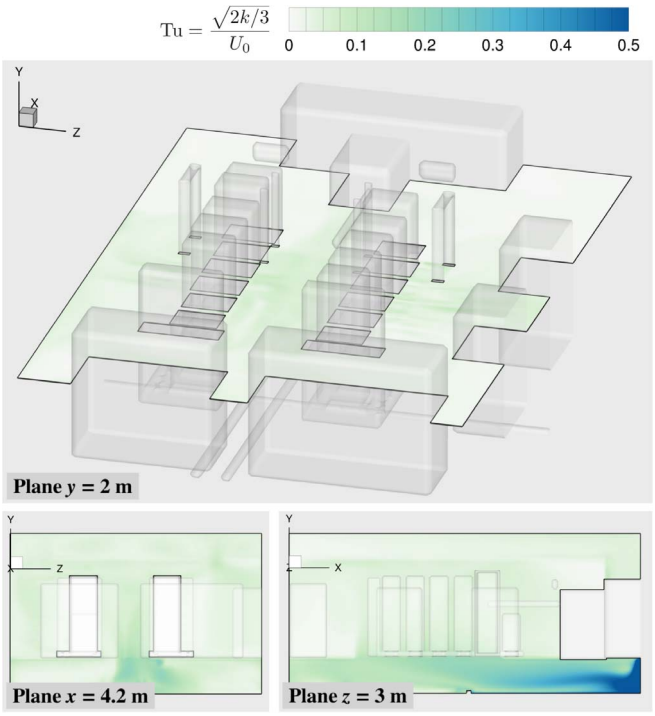

Fig. 10. Turbulence intensity Tu inside CEETHERM, for three different views.

Table 4
Steady and fluctuating total Exergy Destruction (W).

$\iiint \dot{\Psi}'''_{d,\overline{D}}$	$\iiint \dot{\Psi}'''_{d,D'}$	$\iiint \dot{\Psi}'''_{d,\overline{C}}$	$\iiint \dot{\Psi}'''_{d,C'}$
1.11	737.47	12.46	1277.1

[1] For interpretation of color in 'Fig. 11', the reader is referred to the web version of this article.

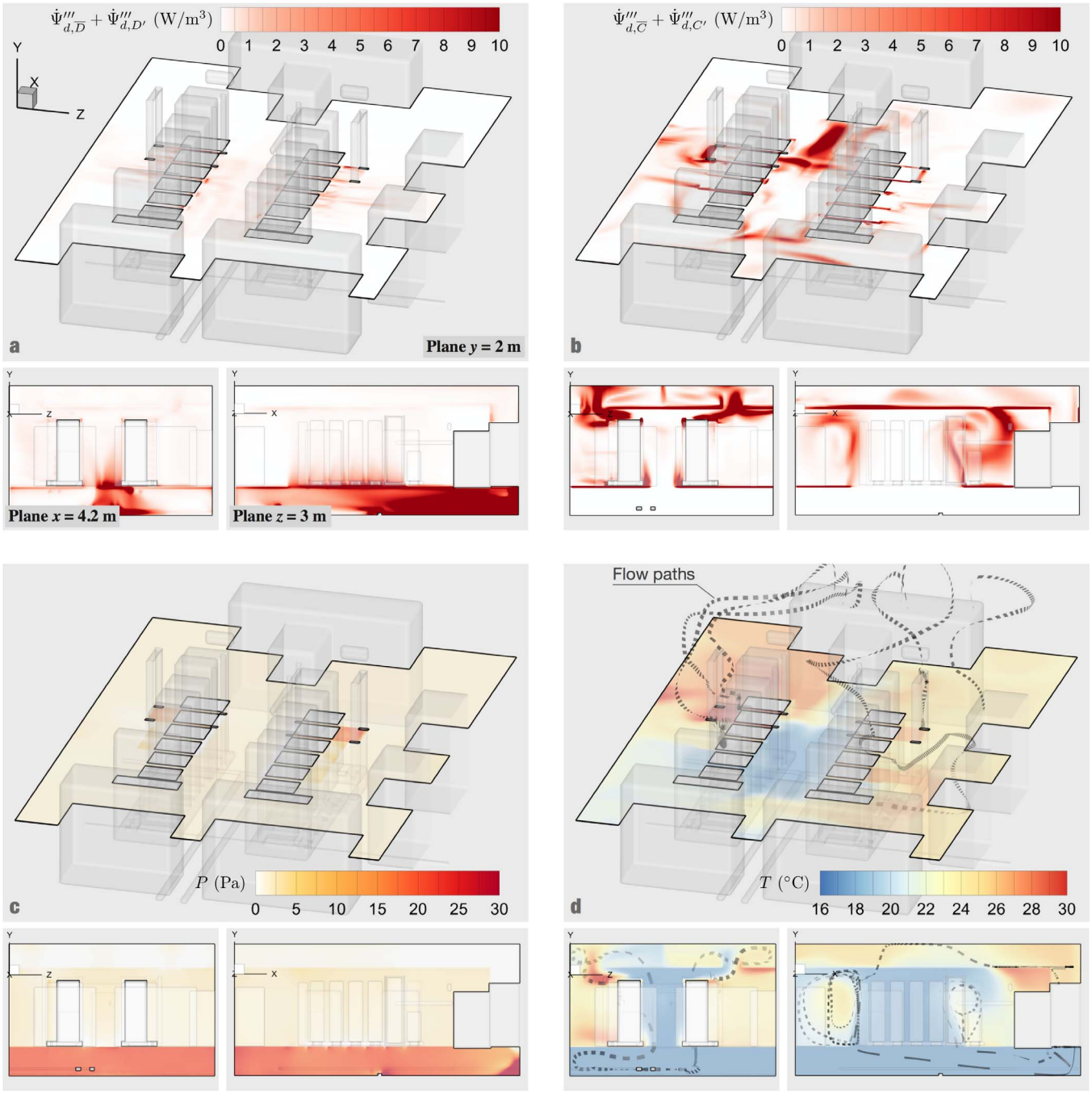

Fig. 11. (a) Exergy Destruction due to Viscous Dissipation ($\dot{\Psi}'''_{d,\overline{D}} + \dot{\Psi}'''_{d,D'}$); (b) Exergy Destruction due to Heat Transfer ($\dot{\Psi}'''_{d,\overline{C}} + \dot{\Psi}'''_{d,C'}$); (c) temperature field; (d) pressure field. Same views as Fig. 9.

5.2. Overall Airside Exergy Destruction

The Exergy flow diagram shown in Fig. 12 sets the scope of this work–namely the non-trivial airside Exergy Destruction calculation–into perspective. Although the Exergy diagram depicts a schematic representation, the width of the arrows resembles the Exergy magnitude at the inlets and outlets, including the Exergy Destruction which fades into a darker gray. Assuming that inside the racks and servers the flow behaves similarly to the study case in Section 3.5, we can safely neglect the turbulent flux terms inside those components, such that:

$$\dot{\Psi}_{d,\text{Racks}} = \underbrace{\sum\nolimits_{\text{Racks}} \left[\left(1-\frac{T_0}{T_s}\right)\dot{Q}_s\right]}_{\dot{\Psi}_{\dot{Q}_{\text{Racks}}}} + \sum_{\text{in}} (\dot{m}\psi) - \sum_{\text{out}} (\dot{m}\psi) \tag{25}$$

$$\dot{\Psi}_{d,\text{CRAC}} = \underbrace{\left(1-\frac{T_0}{T_c}\right)\dot{Q}_{\text{CRAC}}}_{\dot{\Psi}_{\dot{Q}_{\text{CRAC}}}} + (\dot{m}\psi)_{\text{in}} - (\dot{m}\psi)_{\text{out}} \tag{26}$$

where $\psi = c_p(T-T_0) - T_0[c_p \ln(T/T_0) - R\ln(P/P_0)]$ and T_c is the CRAC coolant temperature. The server temperature T_s was estimated as described by Demetriou et al. [44].

The total airside Exergy Destruction is obtained from integrating Eq. (12) over the room volume V_{room}:

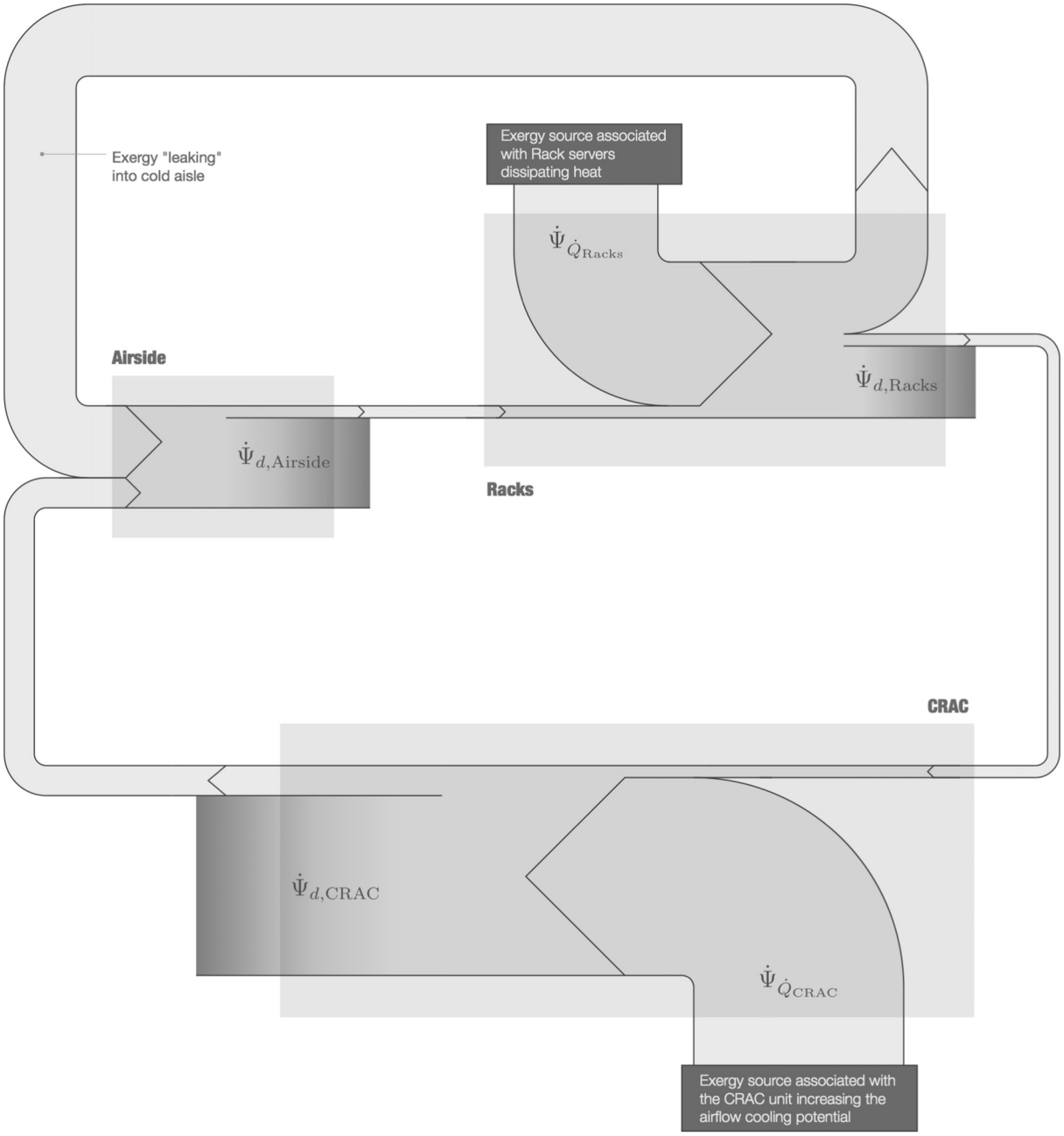

Fig. 12. Airflow Exergy diagram for the data center laboratory CEETHERM.

$$\dot{\Psi}_{d,\mathrm{Airside}} = T_0 \iiint_{V_{\mathrm{room}}} \dot{S}'''_{gen}\, \mathrm{d}V \tag{27}$$

The main mechanisms that destroy Exergy in the airflow as it interacts with each component list as follows:

(i) Airside: We simplify the phenomena (described in Section 5.1) as though the air exiting the CRAC and leaking from the Racks entered an adiabatic mixing chamber. The cooling air pre-mixing with the airflow exiting the rack destroys Exergy due to the heat transfer generated by the streams temperature difference. The combined stream enters the rack with a lower cooling capacity, since its temperature is higher than the cooling flow prior mixing. Moreover, viscous dissipation (pressure drop) irreversibilities occur due to the cooling flow exiting the CRAC that rapidly turns its direction, as well as the sudden expansion the flow suffers when passing through the tiles (Fig. 11(a) and (c)).

(ii) Racks: The assumptions consider the Exergy transported by the airflow that enters and exits the racks, neglecting the inflow and outflow of turbulence flux. The heat transferred from the electronics acts as a major Exergy source, $\dot{\Psi}_{\dot{Q}_{\mathrm{Racks}}}$ in Eq. (25), mostly by raising the air temperature, which in turn destroys Exergy (mainly) due to the heat diffusion that occurs between the server and air. Improving the thermal contact between the server electronics and the cooling flow (heat sinks, heat pipes, packaging) decreases the temperature difference between them, thereby reducing $\dot{\Psi}_{d,\mathrm{Racks}}$.

(iii) CRAC: The cooling unit increases the airflow Exergy, $\dot{\Psi}_{\dot{Q}_{\mathrm{CRAC}}}$ in Eq. (26), by bringing its temperature below T_0, which increases the air cooling capacity. The heat transfer between the coolant and the air dominates the destruction of Exergy. More efficient heat exchange reduces $\dot{\Psi}_{d,\mathrm{CRAC}}$, in other words, improving the cooling units heat exchanger effectiveness minimizes the irreversibilities [38].

This paper focuses on the estimation of mixing and raised floor

Table 5
Exergy Destruction (W) in the airflow as it passes the different stages in the data center.

Airside	Racks	CRAC
2028.1	1620.0	2248.5

Exergy Destruction; analyses of the complete energy flow in data centers are available in [14,24,35,45]. The airspace Exergy Destruction encompasses a significant proportion of the total (Table 5) and simple implementations such as cold aisle containment mitigate (or eliminate) those inefficiencies; in other words, moderate re-designs achieve respectable energy savings. Table 5 also responds to the questions posed in the abstract since the energy savings are considerable, and consequently air flow management improvements are worth the effort.

In recent years, localized cooling emerged as another way to improve the data center thermal efficiency by bringing the heat exchange closer to the servers, commonly in three ways: (a) Over-head cooling, where the cooling units (heat exchangers) usually locate on top of the cold aisle, advecting a downward cold flow near the rack inlets; (b) In-row cooling, where the heat exchangers locate in-between racks, also delivering a cold stream into the cold aisle; (c) Rear-door cooling, where the units locate at the back of the racks, capturing and treating the exiting hot air in situ, thus reducing the occurrence of thermal short-circuiting. Although localized cooling seldom replaces the whole perimeter cooling system, it helps alleviating pressure loads in the raised floor and reducing hot–cold air mixing.

5.3. Anticipating sizable pressure drop inefficiencies via the Irreversibility Distribution Ratio

Generally in convective heat transfer analyses the dissipation of energy due to viscous friction ($\mu\Phi$) represents a negligible part of the total energy. Bejan [40] used length scale analysis to develop a ratio between fluid friction and heat transfer as follows:

$$\left(\frac{\text{fluid friction}}{\text{heat transfer}}\right)_{1st\ law} \sim \frac{\mu(\mathrm{v}^*)^2}{\lambda\,\Delta T^*} \tag{28}$$

The superscript "$*$" denotes the characteristic scale that corresponds to the physics of the problem. Analogously, the ratio between friction irreversibilities and heat transfer irrevesibilities yields:

$$\left(\frac{\text{fluid friction}}{\text{heat transfer}}\right)_{2nd\ law} \sim \frac{T^*}{\Delta T^*}\frac{\mu(\mathrm{v}^*)^2}{\lambda\,\Delta T^*} \tag{29}$$

In most cases, the ratio in (28) is negligibly small; however, the expression in (29) contains the factor $T^*/\Delta T^*$ which might bring this second law ratio closer to unity.

Bejan [40] introduced the irreversibility distribution ratio ϕ and the Bejan number Be as:

$$\phi \equiv \frac{\dot{S}'''_{gen}(\text{fluid friction})}{\dot{S}'''_{gen}(\text{heat transfer})} \tag{30}$$

$$\mathrm{Be} \equiv (1+\phi)^{-1} \tag{31}$$

Eq. (30) shows that when the heat transfer irreversibilities dominate, Be approaches one, whereas in the opposite case, Be approaches zero as the friction irreversibilities become considerable in magnitude.

The irreversibility distribution ratio ϕ for CEETHERM was estimated using v^* as the mean velocity passing through the tiles, $T^* = T_0$ and ΔT^* being the difference between the averaged T entering the CRAC unit and T in the raised floor, resulting in $\phi \approx 0.07$. In comparison, we observed in the study case (Fig. 6) that when $\phi \approx 0.1$, viscous dissipation (pressure drop) effects became non-negligible, leading to a positive slope in the graph. This similarity in the order of magnitude of ϕ between CEETHERM and the study case reinforces the idea that, in data center applications, the Exergy Destruction due to viscous dissipation can be an important source of irreversibilities, as demonstrated by Table 4.

Fig. 11 proved that large pressure drops and cold air inadequately utilized in rack cooling, dominated the inefficiencies in the data center airside. This behavior could have been inferred, at least qualitatively, from the fluid flow and temperature fields without the use of Ψ'''_d, although such an approach provides no information of the magnitude of the energy losses.

The technique presented in this paper complements the convenience of CFD analyses in data center thermal management. A designer can more accurately estimate the energy impact of improved data center configurations by computing the Exergy Destruction; a system that destroys less Exergy utilizes its cooling power consumption more efficiently.

6. Conclusions

In this work we computed the Exergy Destruction from turbulent CFD simulations as a way to localize and quantify wasteful energy usage in a legacy perimeter cooled data center. The relevant conclusions list as follows:

(i) Using an Exergy Destruction analysis we identified zones with significant inefficiencies, and unambiguously quantified energy losses in the data center airside, driven by inadequate delivery of server air cooling and significant pressure drop in the raised floor.
(ii) Contrasting the different Exergy Destruction sources in the system (Airside, Racks, CRAC), we found that the Airside accounted for an important portion of the total Exergy losses. This implies that simple re-designs such as aisle containment and localized cooling can significantly improve the system energy efficiency. In other words, the magnitude of the energy savings justifies any improvement in cooling air delivery.
(iii) Comparing the two Exergy Destruction techniques utilized in this work, the Direct and Indirect method, we concluded that the latter worked well only when the turbulent flux terms are negligible, assumption that invalidates in data center airflow. This implied that the Direct Method proved more suitable to compute the Exergy Destruction inside the data center airside.
(iv) Ignoring the viscous dissipation terms–as commonly assumed in first law analyses–might lead to underestimating the overall Exergy Destruction, especially by neglecting the large pressure drop effects present in the raised floor. The Irreversibility Distribution Ratio helps anticipating whether viscous dissipation plays a role upon the overall inefficiencies.
(v) Generalizing the Direct Method to dynamic (transient) scenarios requires no modification to the formulation as described in this paper, despite the steady state nature of the two problems presented. We acknowledge that during their operation data centers behave dynamically, thus future investigations should point in that direction. Predictive control in thermal management lays at the cutting edge of data center research, and we envision that the tool presented in this paper will contribute towards energy efficient practices.

Acknowledgment

This material is based upon work supported by the National Science Foundation Center for Energy Smart Electronic Systems (ES2) under Grant No. IIP-1134810. Any opinions, findings, and conclusions or recommendations expressed in this material are those of the author(s) and do not necessarily reflect the views of the National Science Foundation. This work was also partially sponsored by CONICYT-Chile under project FONDECYT 11160172. We also thank the GATech data center laboratory CEETHERM for providing empirical and numerical data.

References

[1] Van Heddeghem W, Lambert S, Lannoo B, Colle D, Pickavet M, Demeester P. Trends in worldwide ICT electricity consumption from 2007 to 2012. Comput Commun 2014;50:64–76.
[2] Khalid R, Wemhoff AP, Joshi Y. Energy and exergy analysis of modular data centers. IEEE Trans Compon Pack Manuf Technol 2017;7(9):1440–52.
[3] Nada SA, Said MA. Effect of CRAC units layout on thermal management of data center. Appl Therm Eng 2017;118(Suppl C):339–44.
[4] Chainer TJ, Schultz MD, Parida PR, Gaynes MA. Improving data center energy efficiency with advanced thermal management. IEEE Trans Compon Pack Manuf Technol 2017;7(8):1228–39.
[5] Tatchell-Evans M, Kapur N, Summers J, Thompson H, Oldham D. An experimental and theoretical investigation of the extent of bypass air within data centres employing aisle containment, and its impact on power consumption. Appl Energy 2017;186(Part 3):457–69.
[6] Fouladi K, Wemhoff AP, Silva-Llanca L, Abbasi K, Ortega A. Optimization of data center cooling efficiency using reduced order flow modeling within a flow network modeling approach. Appl Therm Eng 2017;124:929–39.
[7] Ham S-W, Jeong J-W. Impact of aisle containment on energy performance of a data center when using an integrated water-side economizer. Appl Therm Eng 2016;105(Suppl C):372–84.
[8] Agrawal A, Khichar M, Jain S. Transient simulation of wet cooling strategies for a data center in worldwide climate zones. Energy Build 2016;127(Suppl C):352–9.
[9] Habibi Khalaj A, Scherer T, Halgamuge SK. Energy, environmental and economical saving potential of data centers with various economizers across australia. Appl Energy 2016;183(Suppl C):1528–49.
[10] Habibi Khalaj A, Scherer T, Siriwardana J, Halgamuge SK. Multi-objective efficiency enhancement using workload spreading in an operational data center. Appl Energy 2015;138(Suppl C):432–44.
[11] Ham S-W, Kim M-H, Choi B-N, Jeong J-W. Energy saving potential of various air-side economizers in a modular data center. Appl Energy 2015;138(Suppl C):258–75.
[12] Khalaj AH, Scherer T, Siriwardana J, Halgamuge S. Increasing the thermal efficiency of an operational data center using cold aisle containment. In: 7th International conference on information and automation for sustainability; 2014. p. 1–6.
[13] Priyadumkol J, Kittichaikarn C. Application of the combined air-conditioning systems for energy conservation in data center. Energy Build 2014;68(Part A):580–6.
[14] Zimmermann S, Meijer I, Tiwari MK, Paredes S, Michel B, Poulikakos D. Aquasar: a hot water cooled data center with direct energy reuse. Energy 2012;43(1):237–45.
[15] Zimmermann S, Tiwari MK, Meijer I, Paredes S, Michel B, Poulikakos D. Hot water cooled electronics: exergy analysis and waste heat reuse feasibility. Int J Heat Mass Transf 2012;55(23):6391–9.
[16] Rambo J, Joshi Y. Convective transport processes in data centers. Numer Heat Transf Part A: Appl 2006;49(10):923–45.
[17] Herrlin MK. Rack cooling effectiveness in data centers and telecom central offices: the rack cooling index (RCI). ASHRAE-Trans 2005;111(2):725–31.
[18] Song Z. Numerical investigation for performance indices and categorical designs of a fan-assisted data center cooling system. Appl Therm Eng 2017;118(Suppl C):714–23.
[19] Almoli A, Thompson A, Kapur N, Summers J, Thompson H, Hannah G. Computational fluid dynamic investigation of liquid rack cooling in data centres. Appl Energy 2012;89(1):150–5.
[20] Uddin M, Rahman AA. Energy efficiency and low carbon enabler green it framework for data centers considering green metrics. Renew Sustain Energy Rev 2012;16(6):4078–94.
[21] Abdelmaksoud WA, Khalifa HE, Dang TQ, Elhadidi B, Schmidt RR, Iyengar M. Experimental and computational study of perforated floor tile in data centers. In: 2010 12th IEEE intersociety conference on thermal and thermomechanical phenomena in electronic systems; 2010. p. 1–10.
[22] Patankar SV. Airflow and cooling in a data center. J Heat Transf 2010;132(7). 073001.
[23] Samadiani E, Joshi Y. Proper orthogonal decomposition for reduced order thermal modeling of air cooled data centers. J Heat Transf 2010;132(7). 071402.
[24] Shah AJ, Carey VP, Bash CE, Patel CD. Exergy analysis of data center thermal management systems. J Heat Transf 2008;130(2):021401.
[25] Iyengar M, Schmidt RR. Analytical modeling of energy consumption and thermal performance of data center cooling systems: from the chip to the environment. In: ASME 2007 InterPACK conference collocated with the ASME/JSME 2007 thermal engineering heat transfer summer conference, no. 42770; 2007. p. 877–86.
[26] Bash CB, Patel CD, Sharma RK. Dynamic thermal management of air cooled data centers. In: Thermal and thermomechanical proceedings 10th intersociety conference on phenomena in electronics systems, 2006. ITHERM 2006; 2006. p. 8, 452.
[27] Shrivastava SK, Sammakia BG, Schmidt R, Iyengar M, Gilder JWV. Experimental-numerical comparison for a high-density data center: Hot spot heat fluxes in excess of 500 W/FT2. In: Thermal and thermomechanical proceedings 10th intersociety conference on phenomena in electronics systems, 2006. ITHERM 2006; 2006. p. 402–11.
[28] Bhopte S, Agonafer D, Schmidt R, Sammakia B. Optimization of data center room layout to minimize rack inlet air temperature. J Electron Pack 2006;128(4):380–7.
[29] Boucher TD, Auslander DM, Bash CE, Federspiel CC, Patel CD. Viability of dynamic cooling control in a data center environment. J Electron Pack 2005;128(2):137–44.
[30] Sharma R, Bash C, Patel C, Beitelmal M. Experimental investigation of design and performance of data centers. In: The ninth intersociety conference on thermal and thermomechanical phenomena in electronic systems (IEEE Cat. No. 04CH37543), vol. 1; 2004. p. 579–85.
[31] McAllister S, Carey VP, Shah A, Bash C, Patel C. Strategies for effective use of exergy-based modeling of data center thermal management systems. Microelectron J 2008;39(7):1023–9.
[32] Shah AJ, Patel CD. Designing environmentally sustainable electronic cooling systems using exergo-thermo-volumes. Int J Energy Res 2009;33(14):1266–77.
[33] Shah A, Bash C, Patel C. Optimizing data center cooling infrastructures using exergothermovolumes. 2010 12th IEEE intersociety conference on thermal and thermomechanical phenomena in electronic systems (ITherm). IEEE; 2010. p. 1–10.
[34] Bhalerao A, Fouladi K, Silva-Llanca L, Wemhoff AP. Rapid prediction of exergy destruction in data centers due to airflow mixing. Numer Heat Transf Part A: Appl 2016:1–16.
[35] Díaz AJ, Cáceres R, Cardemil JM, Silva-Llanca L. Energy and exergy assessment in a perimeter cooled data center: the value of second law efficiency. Appl Therm Eng 2017;124:820–30.
[36] Herwig H, Kock F. Direct and indirect methods of calculating entropy generation rates in turbulent convective heat transfer problems. Heat Mass Transf 2007;43(3):207–15.
[37] Kock F, Herwig H. Local entropy production in turbulent shear flows: a high-Reynolds number model with wall functions. Int J Heat Mass Transf 2004;47(10):2205–15.
[38] Bejan A. Advanced engineering thermodynamics. Wiley; 2006.
[39] Herwig H. The role of entropy generation in momentum and heat transfer. Trans ASME-C-J Heat Transf 2012;134(3):031003.
[40] Bejan A. Entropy generation minimization: the method of thermodynamic optimization of finite-size systems and finite-time processes vol. 2. CRC Press; 1996.
[41] Sparrow E, Lin S. Turbulent heat transfer in a parallel-plate channel. Int J Heat Mass Transf 1963;6(3):248–9.
[42] Sundaralingam V, Dumler J. Evaluating 6sigmaDC room lite CFD results using temperature measurements of the CEETHERM data center laboratory environment. Tech rep. Atlanta (GA): Internap Network Service; 2012.
[43] Schlichting H, Gersten K, Krause E, Oertel H. Boundary-layer theory vol. 7. Springer; 1955.
[44] Demetriou DW, Erden HS, Khalifa HE, Schmidt RR. Development of an IT equipment lumped capacitance parameter database for transient data center simulations. 2014 IEEE intersociety conference on thermal and thermomechanical phenomena in electronic systems (ITherm). IEEE; 2014. p. 1330–7.
[45] Breen TJ, Walsh EJ, Punch J, Shah AJ, Bash CE. From chip to cooling tower data center modeling: influence of server inlet temperature and temperature rise across cabinet. J Electron Pack 2011;133(1):011004.